

NANO LETTERS

Continued Growth of Single-Walled Carbon Nanotubes

Yuhuang Wang,^{†,‡} Myung Jong Kim,^{†,§} Hongwei Shan,^{†,‡} Carter Kittrell,^{†,‡}
Hua Fan,^{†,§} Lars M. Ericson,^{†,§} Wen-Fang Hwang,^{†,§} Sivaram Arepalli,^{||}
Robert H. Hauge,^{†,‡} and Richard E. Smalley^{*,†,‡,§}

Center for Nanoscale Science and Technology, Carbon Nanotechnology Laboratory, Department of Chemistry, and Department of Physics, Rice University, MS-100, P.O. Box 1892, Houston, Texas 77251-1892, and G. B. Tech./NASA Johnson Space Center, 2101 NASA Road One, Houston, Texas 77058

Received December 23, 2004; Revised Manuscript Received January 23, 2005

ABSTRACT

We demonstrate the continued growth of single-walled carbon nanotubes (SWNTs) from ordered arrays of open-ended SWNTs in a way analogous to epitaxy. Nanometer-sized metal catalysts were docked to the SWNT open ends and subsequently activated to restart growth. SWNTs thus grown inherit the diameters and chirality from the seeded SWNTs, as indicated by the closely matched frequencies of Raman radial breathing modes before and after the growth.

Whether a pristine single-walled carbon nanotube (SWNT) conducts electrons as a quantum wire^{1–3} or behaves as an exceptional semiconductor^{4–6} is determined by its diameter and chiral angle, uniquely indexed with two integers (n,m).⁷ The wide variety of achievable diameters and chiral angles, and their associated properties, make it possible to select tubes of exactly the right kind for optimized performance; however, controlling their (n,m) structure during manufacturing is currently a grand challenge. Although SWNTs are produced with a variety of methods such as arc discharge,^{8,9} laser ablation,¹⁰ and chemical vapor deposition (CVD),^{11–17} none is capable of precisely controlling both the tube

diameter and chirality.¹⁶ In the case of CVD, the most frequently studied method of growth, SWNT diameters are often found to correlate strongly with the diameter of the metal particles from which they are nucleated.^{11–15} However, even starting with metal clusters of identical structure, the growths show no specific control over the chiral angles.¹⁵ Here, we demonstrate the continued growth of seeded SWNTs in a way analogous to epitaxy. By starting with a seeded SWNT, our approach bypasses the nanotube nucleation step. Instead, SWNTs restart the growth as an extension of the existing SWNTs and therefore inherit the same diameter and chirality from the starting SWNTs. The ability to separate the typically inefficient nucleation step from the growth of SWNTs, and to restart the growth, coupled with the continuing advances toward type-specific chemistry/separation of SWNTs,^{18–22} opens the possibility of amplifying SWNTs with only the desired (n,m)s.

* Corresponding author. E-mail: smalley@rice.edu; Telephone: (01)-713-348-3250; Fax: (01)-713-348-5320.

[†] Carbon Nanotechnology Laboratory, Rice University.

[‡] Department of Chemistry, Rice University.

[§] Department of Physics, Rice University.

^{||} NASA Johnson Space Center.

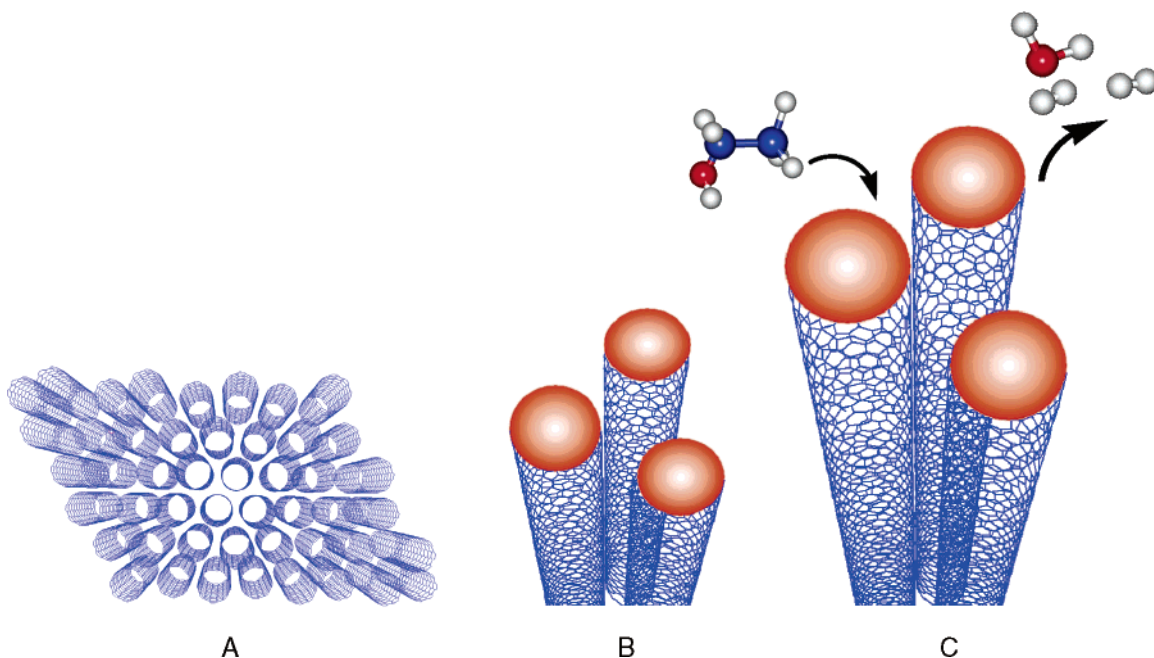


Figure 1. Schematic illustration of the continued growth of SWNTs: (A) preparing an ordered array of open-ended SWNTs, (B) reductively docking transition metal nanoparticles as a catalyst to the nanometer-sized open ends, and (C) activating the docked catalysts and introducing carbon feedstock such as ethanol to grow epitaxially.

Figure 1 illustrates the three stages of our experiments: (1) preparing an ordered array of open-ended SWNTs; (2) reductively docking transition metals as a catalyst to the nanometer-sized open ends; and then (3) heating to 700–850 °C in the presence of a carbon feedstock such as ethanol or ethylene. To prepare an ordered array of open-ended SWNTs, we spun SWNTs of finite length into a continuous, aligned, neat fiber,²³ microtomed the fiber to obtain a flat surface, etched SWNTs homogeneously, without differentiating the sidewalls and the ends, and then removed surface contaminants on SWNTs while keeping the ends open. This produces a clean – largely free of amorphous carbon, oxides, and metal residues – SWNT substrate with open-ended SWNTs aligned along the fiber axis.

The neat SWNT fibers, containing no surfactant or polymer, were made by spinning a 8 wt % dispersion of purified HiPco material in 102% sulfuric acid (with 2 wt % excess SO₃) into an ether coagulant.²³ A 60 cm length of fiber, hanging in space with only the two ends glued to a quartz boat, was annealed stepwise at 110 °C, 350 °C, 900 °C, and then cooled to 800 °C and room temperature, holding at each temperature for 3 h in a flow of 20 sccm H₂ and 740 sccm Ar (both 99.999% purity). The annealing completely removed residual sulfuric acid and improved the mechanical strength of the fiber. Further rinsing with hydrochloric acid reduced the residual metals, which migrated to the surface, to a trace level (<0.2 at. %), as determined by energy-dispersive X-ray analysis. The fiber possessed a polarization Raman ratio about 20:1, suggesting excellent alignment of SWNTs along the fiber axis.²³

To achieve a flat surface, a ~10 mm length of SWNT neat fiber was embedded in a 2.3 M sucrose solution, frozen to –100 °C, and microtomed perpendicular to the fiber axis with a diamond knife (DiATOME).²⁴ After microtoming, the

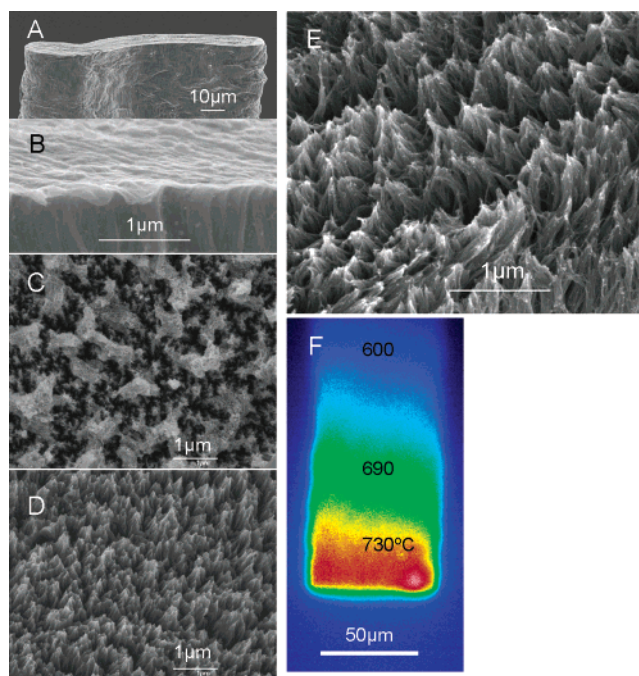


Figure 2. Preparation of an ordered array of open-ended SWNTs. (A) A flat surface created by microtoming perpendicular to the fiber axis of a SWNT neat fiber. (B) The edge of the microtomed surface showing nanotubes combed along the cutting direction. The combed layer was etched with atomic oxygen (C), and removed with hydrochloric acid to give a macroscopic surface of open-ended SWNTs (D). The surface was further cleaned by heating with 0.32 Torr H₂ at ~730 °C for 30 min. A thin layer (4.2 Å) Fe–Ni (50–50 wt %) was deposited on the surface to facilitate the removing of carbon oxides. The exposed metals were removed with acid to give a clean substrate with open-ended SWNTs aligned along the normal to the substrate (E). (F) A glowing SWNT fiber with temperature determined from integrated blackbody radiation.

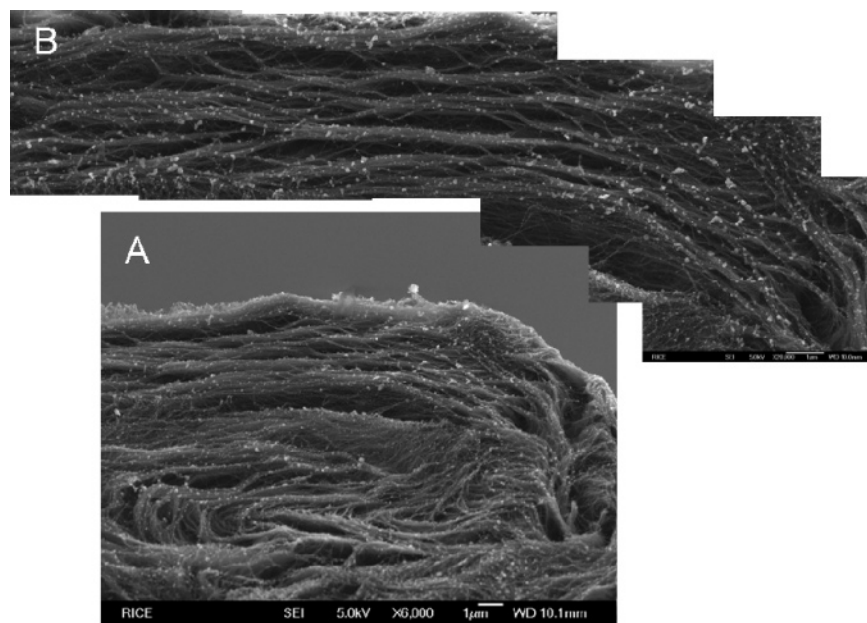


Figure 3. Continuous ropes ($\sim 25 \mu\text{m}$) sprout from an edge of a SWNT substrate after growing with $\text{C}_2\text{H}_5\text{OH}$ at 800°C . The sample was heated to 700°C within seconds with the 488 nm output of an Ar^+ laser.

remaining fiber was recovered intact, rinsed with deionized water to remove sucrose, and then mounted onto a stainless steel hypodermic needle, with the microtomed end protruding $2\text{--}3 \text{ mm}$ for subsequent processing. Conductive silver paint was used to secure the fiber and to ensure good electric contact. The diamond knife did not apparently “cut” the tubes, but instead combed the fibrils along the cutting direction, producing a layer only $20\text{--}50 \text{ nm}$ thick with almost perfect alignment (Figure 2B). Given the unrivaled hardness and the extreme sharpness (radius of curvature $< 2 \text{ nm}$) of the diamond knife, this combing effect constitutes a direct visualization of the exceptional toughness and stiffness of SWNTs, similar to previous observation with a multiwall carbon nanotubes/epoxy composite.²⁵

The combed layer was etched with atomic oxygen generated by UV photon-dissociation of ozone or by inductive-coupled plasma.²⁴ The resulting debris and exposed residual metal were subsequently removed with 1 N hydrochloric acid (Figure 2D). In contrast with O_2 and H_2 , atomic oxygen etched SWNTs at near unity efficiency with almost no differentiation of sidewalls and ends, thereby leaving oxidized sidewalls, if exposed, and presumably open ends terminated with oxygen containing functional groups such as carboxylic acid and quinone. To remove the sidewall oxides, we deposited a thin layer (4.2 \AA) Fe–Ni ($50\text{--}50 \text{ wt } \%$) alloy onto the surface as a H_2 dissociation catalyst and subsequently heated the surface to 730°C in 0.32 Torr H_2 for 30 min .²⁶ While H_2 alone was capable of removing these surface oxides, the deposited metal catalyst lowered the effective reaction temperature by $\sim 100^\circ\text{C}$. This placed the open ends at a temperature lower than 800°C , where open-ended SWNTs remain open as evidenced by the Xe absorption capacity 280 times that of a close-ended SWNT sample.^{27,28} The exposed residual metals were removed with hydrochloric acid to give a clean SWNT array with open ends readily exposed for the reductive docking (Figure 2E).

To dock a metal nanoparticle onto the open end of a SWNT, we took advantage of the structural difference between the sidewall and the open end of an SWNT. The sidewall, like the graphite basal plane, is chemically inert to most metals.²⁹ A vapor deposited metal atom (Fe or Ni) diffuses at room temperature until it encounters an open end (if no other surface defects exist) to which it can bond strongly ($\sim 2\text{--}3 \text{ eV}$) and form a nucleation center. Subsequent atoms bond to these nucleation centers and grow into clusters sufficiently large to serve as the catalyst for the continued growth of SWNTs. Typically, a thin layer (2.1 \AA) of Fe–Ni $50\text{--}50 \text{ wt } \%$ alloy was e-beam-evaporated onto the SWNT substrate. During the deposition, the substrate was kept at $300\text{--}350^\circ\text{C}$ in $5 \times 10^{-6} \text{ Torr H}_2$ to allow the metal atoms to diffuse. After deposition, most metal particles were observed accumulating at the SWNT ends and step-edges along ropes, with a size equal to or less than the scanning electron microscopy (SEM) resolution limit of $\sim 3 \text{ nm}$. The metal particle attached to the SWNT end digests the SWNT along its length, during which it may adapt itself to the structure of the open end in a process we term “reductive docking.”

After the reductive docking, the continued growth was started by a smooth transition from a H_2/Ar environment to a growth environment while keeping the SWNTs at the growth temperatures, or alternatively, by a rapid heating to the desired growth temperature in just $0.5\text{--}3 \text{ min}$, immediately following the introduction of carbon feedstock. Both of these strategies were aimed to active the SWNT/catalyst integrity to mimic a growing SWNT in the HiPco process.³⁰

Figure 3 shows SEM images of an edge of a macroscopic array of open-ended SWNTs after growth using $\text{C}_2\text{H}_5\text{OH}$ as feedstock. The morphology of the surface changed significantly after growth, which was not observed for samples heated in just H_2 . Figure 3B shows loose SWNT ropes

sprouting from an edge of a macroscopic array of SWNTs and undulate along the substrate for over 25 μm before an apparent end could be found. The sample shows a rougher surface than before growth, with ropes sticking out from the microtomed surface up to 1.7 μm in length. In every case, the nanotube ropes were found rooted to the existing nanotubes and tended to maintain the orientation of their seeds, although different ropes often grew along different directions. We suspect that these ropes originally grew along the fiber axis, but fell over onto the plane of the substrate midway through their growth. This explanation is supported by the observation of rapid extension of the incandescence (viewed by the CCD camera) in various regions during the first 5–20 min of growth, while the overall extension of the incandescence was much slower. The termination of growth was likely caused by two mechanisms. As a nanotube falls over onto the substrate, its growth path can be blocked easily by other tubes and particles. As the nanotube grows away from the substrate, it is cooled by the increasing collisions with the cold feed gases that cannot be heated directly by the Ar^+ laser beam. Both mechanisms could terminate the growth. We believe, however, that the growth should never stop if the growing SWNTs are packed in an array such that each tube is in side-by-side van der Waals contact with six others and the “live” end of the tube is always exposed and free to grow.

To prove that these new ropes are continued growth of the existing SWNTs, we characterize the new ropes, as opposed to the starting SWNT arrays, with a Raman microscope (Renishaw Micro-Raman System 1000). Three laser excitation lines (514.5, 633, and 780 nm) were used to cover a broad range of (n,m) , each of which is shown as a point in the Kataura plot.³¹ All Raman spectra were obtained using an 1800 grooves/mm grating, with a corresponding spectral resolution better than 0.7, 1.2, and 1.8 cm^{-1} for 780, 633, and 514.5 nm, respectively. To enhance the Raman signal from the restarted growth, we took advantage of the anisotropic polarization of SWNTs³² by aligning the polarization of the incident laser light parallel to the new ropes. These ropes showed a parallel-to-perpendicular Raman ratio of $\sim 3:1$, whereas the underlying starting SWNT arrays, which were perpendicular to the new ropes, gave a ratio typically between 1.1:1 and 1.3:1, slightly deviating from the expected 1:1 because of small tilt angles between the incident light and the fiber axis. The difference between the two ratios, amounting to over 56% Raman signal, was therefore attributed to the new growth.

None of our Raman spectra reveal any multiwall carbon nanotubes (MWNTs). The addition of MWNTs would result in a decrease in the G^+/G^- ratio and a blue shift of the G^+ peak if there were as few as 7.6% MWNTs,³³ neither of which is observed in the sample after continued growth. While Raman spectra are not sensitive enough to exclude the growth of MWNTs in our experiments, it is safe to estimate that at least 92% of the Raman signal arises from SWNTs. From the above two estimates, we infer that more than 50% of the Raman signal arises from new SWNTs.

Figure 4 compares the radial breathing modes (RBMs) of Raman spectra before and after growth. Over 150 different

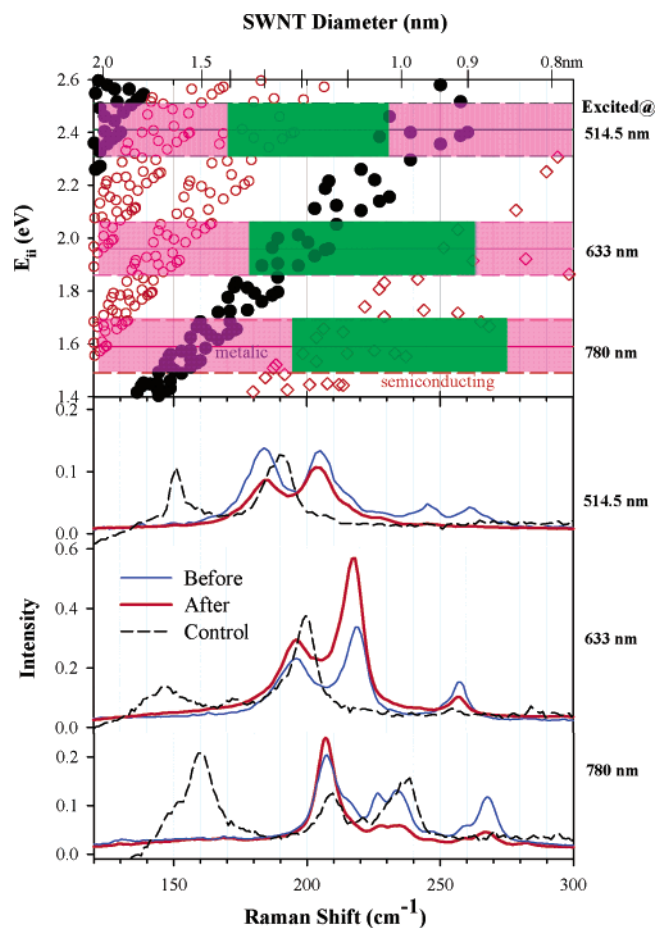


Figure 4. Comparison of Raman spectra (radial breathing modes) before and after the continued growth. The intensity was normalized to the G^+ peak, and the control times two. The control SWNT sample was prepared following Maruyama’s alcohol CVD recipe. The top panel is a Kataura plot of transition energy as a function of nanotube diameter and Raman shift. Circles are from Maruyama,³⁸ and diamonds are from Weisman et al.³⁹ The diameter was calculated by $d(n,m) = 223.5/(\text{RBM} - 12.5)$.⁴⁰ The excited window for each laser line is highlighted with pink. The RBM regions for SWNTs presented in the continued growth sample are highlighted with green.

(n,m) , each shown as a point in the Kataura plot³¹ (Figure 4, top panel), are covered by the three excitation windows. Strikingly, the positions of RBMs after growth closely match up with almost every existing mode from the seeded SWNTs. As the Kataura plot shows, approximately four times more species are within the windows of detection for resonance enhancement of the RBMs (highlighted in green) than were actually observed. Yet after the continued growth process, there is not one single instance of any additional chirality appearing in the RBM spectra for any of the three lasers. Thus, even though catalyst nanoparticles with a wide range of diameters are present, the variety of (larger) diameter SWNTs expected from dominant nucleated growth was not detected. In comparison, SWNT samples prepared following Maruyama et al.’s alcohol CVD recipe,³⁴ whose conditions (growth temperature and feedstock) were closely followed in these continued growth experiments, show the presence of a large portion of SWNTs with relatively larger diameters. Therefore, we rule out spontaneous nucleation as a significant

contribution to the new growth. Further analysis of the Raman spectra shows that SWNTs with larger diameters are more populated after growth. We attribute this shift to preferential growth of larger diameter SWNTs and/or selective removal of smaller diameter SWNTs during the reductive docking process. From each sample 4–7 spots (spot size $\sim 1 \mu\text{m}^2$) were taken for comparison. The RBMs appeared at the same wavenumbers, but the relative intensities varied, suggesting an inhomogeneous growth across the SWNT array. The growth was less dense since not all nanotubes restart growth and therefore the “roping peak” at 267 cm^{-1} was diminished due to less tube–tube contact.³⁵

These Raman results, both the close matching of the RBMs of the new growth with that of the seeded SWNTs and the absence of otherwise inevitable spontaneous nucleation, cannot be explained without invoking the continued growth mechanism, although more details need to be uncovered in future work, such as following the growth of just one individual SWNT. We believe that tip growth is the active mechanism during these SWNT continued growth experiments. After growth, metal particles are frequently observed at the ends of nanotubes (SEM, result not shown), but further work is needed to determine unambiguously the size and chemical state of the catalyst. We argue that with the tip growth mechanism, the growing tips stay exposed, thereby eliminating the diffusion problem that generally occurs when the catalyst is at the base of the nanotube.³⁶ The ability to restart the growth of SWNTs, coupled with the ease of precursor diffusion, opens the opportunity to grow nanotubes, in principle, to unlimited lengths, simply by repeating the process.

While the continued growth experiments were successful under varying carbon precursors and temperatures, the process was sensitive to SWNT surface conditions and extraneous environmental species. Growth was severely retarded in sample areas that had been extensively imaged by a SEM before growth. This effect is attributed to compromised SWNT ends, either because of structure damage from the electron beam and/or unavoidable amorphous carbon surface contamination during SEM. Similarly, annealing the open-ended SWNTs at $1140 \text{ }^\circ\text{C}$ in a vacuum better than 6×10^{-8} Torr for 30 min closed the open ends, which resulted in little growth. The growth with ethanol was extremely sensitive to trace amount of water and oxygen. A minute amount of water ($\sim 1\%$, determined with an online residual gas analyzer) was enough to completely inhibit the growth and even to cause etching of the SWNT substrates.

Given the relatively low surface density of the starting SWNT fiber seed, estimated to be in the range of $10^{12} - 3 \times 10^{13}/\text{cm}^2$, the observation of growing loose ropes in local regions, a phenomenon only possible when a large number of tubes are growing in about the same direction, is encouraging. It suggests a relatively high overall efficiency in the end opening, reductive docking, and catalyst reactivation steps. Further improvement of these processes, in particular the density of the starting arrays of open-ended SWNTs, may allow the synthesis of a continuous crystalline fiber comprising long, parallel nanotubes in an ordered array.

We are optimistic that this pathway, challenging as it may be, will eventually lead to SWNT single crystals of any desired (n,m) – a long sought dream for this field.^{10,37} Nevertheless, a pathway that enables control over both the SWNT diameter and chiral angle during synthesis is now possible.

Acknowledgment. We gratefully acknowledge Steve Ripley and Bruce Brinson for excellent technical support, Dr. John Jones for a LabVIEW controlling program, Drs. Dave Geohagan, Wade Adams, Matteo Pasquali, and Gerry Lavin for helpful communications. This work was supported by DOE (DE-AC05-000R22725), NASA (NCC 9-77), and the Robert A. Welch Foundation (C-0689). Y.W. gratefully acknowledges a Rice Presidential Fellowship and a David G. Nance Award from Nanotechnology Foundation in Texas.

References

- (1) Tans, S. J.; Devoret, M. H.; Dai, H. J.; Thess, A.; Smalley, R. E.; Geerligs, L. J.; Dekker, C. *Nature* **1997**, *386*, 474.
- (2) Kong, J.; Yenilmez, E.; Tomblor, T. W.; Kim, W.; Dai, H.; Laughlin, R. B.; Liu, L.; Jayanthi, C. S.; Wu, S. Y. *Phys. Rev. Lett.* **2001**, *87*, 106801.
- (3) Liang, W.; Bockrath, M.; Bozovic, D.; Hafner, J. H.; Tinkham, M.; Park, H. *Nature* **2001**, *411*, 665.
- (4) Tans, S. J.; Verschuere, A. R. M.; Dekker, C. *Nature* **1998**, *393*, 49.
- (5) Javey, A.; Guo, J.; Wang, Q.; Lundstrom, M.; Dai, H. *Nature* **2003**, *424*, 654.
- (6) Durkop, T.; Brintlinger, T.; Fuhrer, M. S. *AIP Conf. Proc.* **2002**, *633*, 242.
- (7) Saito, R.; Dresselhaus, G.; Dresselhaus, M. S. *Physical Properties of Carbon Nanotubes*; Imperial College Press: London, 1998.
- (8) Bethune, D. S.; Kiang, C. H.; deVries, M. S.; Gorman, G.; Savoy, R.; Vazquez, J.; Beyers, R. *Nature* **1993**, *363*, 605.
- (9) Journet, C.; Maser, W. K.; Bernier, P.; Loiseau, A.; Delachapelle, M. L.; Lefrant, S.; Deniard, P.; Lee, R.; Fischer, J. E. *Nature* **1997**, *388*, 756.
- (10) Thess, A.; Lee, R.; Nikolaev, P.; Dai, H. J.; Petit, P.; Robert, J.; Xu, C. H.; Lee, Y. H.; Kim, S. G.; Rinzler, A. G.; Colbert, D. T.; Scuseria, G. E.; Tomanek, D.; Fischer, J. E.; Smalley, R. E. *Science* **1996**, *273*, 483.
- (11) Zhang, Y.; Li, Y.; Kim, W.; Wang, D.; Dai, H. *Appl. Phys. A* **2002**, *74*, 325.
- (12) Cheung, C. L.; Kurtz, A.; Park, H.; Lieber, C. M. *J. Phys. Chem. B* **2002**, *106*, 2429.
- (13) Li, Y.; Kim, W.; Zhang, Y.; Rolandi, M.; Wang, D.; Dai, H. *J. Phys. Chem. B* **2001**, *105*, 11424.
- (14) Choi, H. C.; Kim, W.; Wang, D.; Dai, H. *J. Phys. Chem. B* **2002**, *106*, 12361.
- (15) An, L.; Owens, J. M.; McNeil, L. E.; Liu, J. *J. Am. Chem. Soc.* **2002**, *124*, 13688.
- (16) Liu, J.; Fan, S.; Dai, H. *MRS Bull.* **2004**, *29*, 244.
- (17) Murakami, Y.; Chiashi, S.; Miyauchi, Y.; Hu, M.; Ogura, M.; Okubo, T.; Maruyama, S. *Chem. Phys. Lett.* **2004**, *385*, 298.
- (18) Chen, Z.; Du, X.; Du, M.-H.; Rancken, C. D.; Cheng, H.-P.; Rinzler, A. G. *Nano Lett.* **2003**, *3*, 1245.
- (19) Zheng, M.; Jagota, A.; Semke, E. D.; Diner, B. A.; McLean, R. S.; Lustig, S. R.; Richardson, R. E.; Tassi, N. G. *Nature Materials* **2003**, *2*, 338.
- (20) Krupke, R.; Hennrich, F.; Loehneysen, H. V.; Kappes, M. M. *Science* **2003**, *301*, 344.
- (21) Strano, M. S.; Dyke, C. A.; Usrey, M. L.; Barone, P. W.; Allen, M. J.; Shan, H.; Kittrell, C.; Hauge, R. H.; Tour, J. M.; Smalley, R. E. *Science* **2003**, *301*, 1519.
- (22) Chattopadhyay, D.; Galeska, I.; Papadimitrakopoulos, F. *J. Am. Chem. Soc.* **2003**, *125*, 3370.
- (23) Ericson, L. M.; Fan, H.; Peng, H.; Davis, V. A.; Zhou, W.; Sulpizio, J.; Wang, Y.; Booker, R.; Vavro, J.; Guthy, C.; Parra-Vasquez, A. N. G.; Kim, M. J.; Ramesh, S.; Saini, R. K.; Kittrell, C.; Lavin, G.; Schmidt, H.; Adams, W. W.; Billups, W. E.; Pasquali, M.; Hwang, W.-F.; Hauge, R. H.; Fischer, J. E.; Smalley, R. E. *Science* **2004**, *305*, 1447.

- (24) Wang, Y. H. *Seed Crystals and Catalyzed Epitaxy of Single-Walled Carbon Nanotubes*; Ph.D. Thesis, Rice University, 2004.
- (25) Ajayan, P. M.; Stephan, O.; Colliex, C.; Trauth, D. *Science* **1994**, *265*, 1212.
- (26) The fiber tip was heated with a 488 nm continuous wave Ar⁺ laser beam (45° incidence angle), which allows almost instant heating to the desired temperature. Temperature was measured by summing the blackbody radiation from 600 to 1100 nm measured with a thermal electronic cooled charge coupled devices (TEA/CCD512K, Princeton Instruments), taking into account the optical property of every component of the homemade optical system. A feedback from the CCD camera was used to stabilize the temperature of the fiber tip by regulating the laser output. This optical system allows simultaneous temperature profile (down to 300 °C, with a systematic error <50 °C due to uncertainty on the spectral emissivity of SWNTs) and spatially resolving (~1 μm) the fiber in real time.
- (27) Kuznetsova, A.; Mawhinney, D. B.; Naumenko, V.; Yates, J. T.; Liu, J.; Smalley, R. E. *Chem. Phys. Lett.* **2000**, *321*, 292.
- (28) Byl, O.; Kondratyuk, P.; Forth, S. T.; FitzGerald, S. A.; Chen, L.; Johnson, J. K.; Yates, J. T., Jr. *J. Am. Chem. Soc.* **2003**, *125*, 5889.
- (29) Zhang, Y.; Franklin, N. W.; Chen, R. J.; Dai, H. *Chem. Phys. Lett.* **2000**, *331*, 35.
- (30) Bronikowski, M. J.; Willis, P. A.; Colbert, D. T.; Smith, K. A.; Smalley, R. E. *J. Vac. Sci. Technol., A* **2001**, *19*, 1800.
- (31) Kataura, H.; Kumazawa, Y.; Maniwa, Y.; Umezu, I.; Suzuki, S.; Ohtsuka, Y.; Achiba, Y. *Synth. Met.* **1999**, *103*, 2555.
- (32) Duesberg, G. S.; Loa, I.; Burghard, M.; Syassen, K.; Roth, S. *Phys. Rev. Lett.* **2000**, *85*, 5436.
- (33) Qian, W.; Liu, T.; Wei, F.; Yuan, H. *Carbon* **2003**, *41*, 1851.
- (34) Murakami, Y.; Miyauchi, Y.; Chiashi, S.; Maruyama, S. *Chem. Phys. Lett.* **2003**, *377*, 49.
- (35) Heller, D. A.; Barone, P. W.; Swanson, J. P.; Mayrhofer, R. M.; Strano, M. S. *J. Phys. Chem. B* **2004**, *108*, 6905.
- (36) Louchev, O. A.; Sato, Y.; Kanda, H. *Appl. Phys. Lett.* **2002**, *80*, 2752.
- (37) Chisholm Matthew, F.; Wang, Y.; Lupini Andrew, R.; Eres, G.; Puzos Alex, A.; Brinson, B.; Melechko Anatoli, V.; Geohegan David, B.; Cui, H.; Johnson Marie, P.; Pennycook Stephen, J.; Lowndes Douglas, H.; Arepalli, S.; Kittrell, C.; Sivaram, S.; Kim, M.; Lavin, G.; Kono, J.; Hauge, R.; Smalley Richard, E. *Science* **2003**, *300*, 1236; author reply 1236.
- (38) Maruyama, S. *Transition Energies from Tight Band Theory*. <http://www.photon.t.u-tokyo.ac.jp/~maruyama/kataura/kataura.html>.
- (39) Weisman, R. B.; Bachilo, S. M. *Nano Lett.* **2003**, *3*, 1235.
- (40) Bachilo, S. M.; Strano, M. S.; Kittrell, C.; Hauge, R. H.; Smalley, R. E.; Weisman, R. B. *Science* **2002**, *298*, 2361.

NL047851F